Organic & Biomolecular Chemistry

Improvement in photodynamic activity by porphyrin–fullerene composite system in lipid membrane

Journal:	*Organic & Biomolecular Chemistry*
Manuscript ID	OB-ART-01-2023-000027.R3
Article Type:	Paper
Date Submitted by the Author:	22-May-2023
Complete List of Authors:	Nishimura, Kotaro; Hiroshima Daigaku, Applied Chemistry Program, Graduate School of Advanced Science and Engineering Yamana, Keita; Hiroshima University, Applied Chemistry Program, Graduate School of Advanced Science and Engineering Kawasaki, Riku; Hiroshima University, Engineering Ikeda, Atsushi; Hiroshima Daigaku, Applied Chemistry Program, Graduate School of Advanced Science and Engineering

ARTICLE

Improvement in photodynamic activity by porphyrin–fullerene composite system in lipid membrane†

Received 00th January 20xx,
Accepted 00th January 20xx

DOI: 10.1039/x0xx00000x

Kotaro Nishimura, Keita Yamana, Riku Kawasaki and Atsushi Ikeda *[a]

Porphyrin–fullerene composite systems are attracting great attention as photodynamic agents; however, water-soluble derivatives are still scarce. Herein, we prepared noncovalently a lipid membrane–incorporated porphyrin–fullerene composite system with relative stability in aqueous solution. As in the case of porphyrin–fullerene composite systems in nonpolar solvents, efficient formation of singlet oxygen occurred via photoinduced energy transfer between porphyrin and fullerene as the predominant pathway in the photodynamic activity under the hydrophobic condition of the lipid membranes, resulting in enhanced photodynamic activity toward Colon26 and HeLa cells compared with the individual porphyrin and fullerene components. Furthermore, the porphyrin–fullerene composite system exhibited high selectivity toward HeLa cells over normal mouse fibroblast L929 cells.

Introduction

Porphyrin–fullerene composite systems,[1–7] in which the porphyrin and fullerene components are connected via covalent bonding or supramolecular interactions, have attracted continuous interest because of their applications as photovoltaic,[8–11] photocatalytic,[12,13] and photodynamic materials.[14–19] The key processes to realize these applications are photoinduced energy transfer and electron transfer, which are significantly influenced by environmental conditions such as solvents. Thus, energy transfer between porphyrin and fullerene is a major process in nonpolar solvents such as cyclohexane, benzene, or toluene, whereas electron transfer is predominant in polar solvents such as acetonitrile or benzonitrile.[2,20,21] In these composite systems, the photodynamic activity may occur via the generation of singlet oxygen ($^1O_2$) through an energy transfer mechanism from porphyrin to fullerene (type II pathway) or by producing superoxide ($O_2^{\bullet-}$) through an electron transfer mechanism (type I pathway) from fullerene to dissolved oxygen (Scheme S1).[22] The generation of $O_2^{\bullet-}$ and hydroxyl radical accompanying with it by Scheme S2[23] via the charge separation induced by electron transfer between porphyrin and fullerene has been proposed as the predominant pathway under physiological conditions.[22] Although some porphyrin–fullerene composite systems have outperformed porphyrin monomers in terms of photodynamic activity,[15–17] water-soluble porphyrin–fullerene composite systems are still scarce because of their high hydrophobicity and tendency to self-aggregate.[15–17] It is very important for biological applications such as photodynamic therapy.

Although a lipid membrane–incorporated tetraphenylporphyrin provided an unstable aqueous solution, we previously reported the preparation of stable aqueous solutions containing lipid membrane–incorporated porphyrin derivatives (LMIPors) such as 5,10,15,20-tetrakis(4-hydroxyphenyl)porphyrin (**1**) and 5,10,15,20-tetrakis(4-aminophenyl)porphyrin[24–26] and lipid membrane–incorporated [60]fullerene derivatives (LMIC$_{60}$s).[27] Furthermore, LMI**1** and lipid membrane–incorporated fullerene derivative C$_{60}$-**2** (LMIC$_{60}$-**2**) have a higher photodynamic activity toward HeLa cells under the photoirradiation at long wavelength (610–740 nm) with high biological tissue permeability (Fig. 1),[26–28]

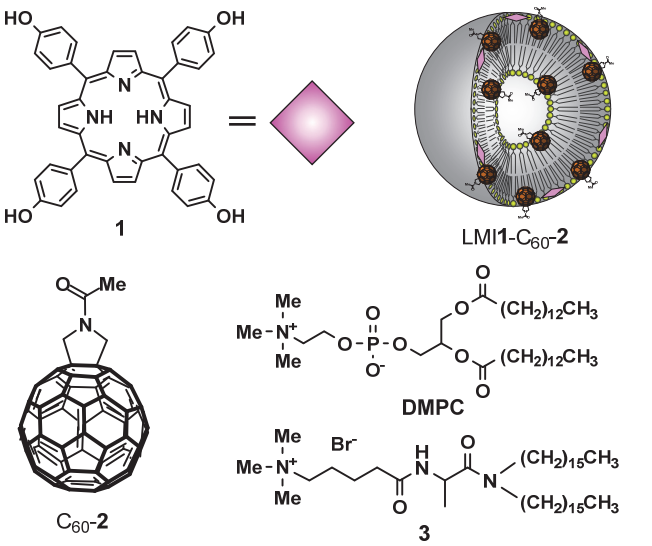

Fig. 1 Structures of porphyrin derivative **1**, [60]fullerene derivative C$_{60}$-**2**, and the lipids DMPC and **3** used to obtain the lipid membrane–incorporated LMI**1**–C$_{60}$-**2** composite system.

Applied Chemistry Program, Graduate School of Advanced Science and Engineering, Hiroshima University, 1-4-1 Kagamiyama, Higashi-Hiroshima, Hiroshima 739-8527, Japan.

† Electronic Supplementary Information (ESI) available: Schemes, ^{1}H NMR, fluorescence and UV–Vis absorption spectra, cell viability and flow cytometry. See DOI: 10.1039/x0xx00000x

because **1** and C_{60}-**2** have high $^1O_2$ generation ability by location near the surface of the lipid membrane.[26,28] On the basis of this work, we herein propose noncovalently a new composite system combining porphyrin derivative **1** and fullerene derivative C_{60}-**2** in liposomes, i.e., a lipid membrane–incorporated LMI**1**–C_{60}-**2** composite system (Fig. 1),[28–32] and describe the investigation of its stability and photodynamic activity compared with those of the individual components LMI**1** and LMIC_{60}-**2**.

Results and discussion

LMI**1** was prepared via an injection method,[33,34] according to which a dimethyl sulfoxide (DMSO) solution of **1** was added to an aqueous solution of 1,2-dimyristoyl-*sn*-glycero-3-phosphocholine (DMPC) liposome, as previously reported (Scheme S3).[26] Meanwhile, LMIC_{60}-**2** and LMI**1**–C_{60}-**2** were prepared following an exchange method of solubilizing agent as shown in Scheme S3,[35–37] in which an aqueous solution of a γ-cyclodextrin–C_{60}-**2** complex[38,39] was added slowly to an aqueous solution containing the DMPC liposome and LMI**1** at 80 °C as described in a previous report.[28] The peak broadening of LMIC_{60}-**2** and LMI**1**–C_{60}-**2** in the UV–Vis absorption spectra compared with the γ-cyclodextrin–C_{60}-**2** complex suggested the transfer of C_{60}-**2** from γ-cyclodextrin to the DMPC liposomes or LMI**1** (Fig. 2), indicating that C_{60}-**2** self-aggregated in the liposomes. Furthermore, the disappearance of the peaks assignable to γ-cyclodextrin from the ^{1}H NMR spectrum of the γ-cyclodextrin–C_{60}-**2** complex after heating at 80 °C for 2 h revealed that all C_{60}-**2** was released from the cavity of γ-cyclodextrin (Fig. S1). The coexistence of **1** and C_{60}-**2** in the liposomes was confirmed by a fluorescence quenching experiment, in which C_{60}-**2** acted as a fluorescence quencher of **1** (Fig. S2). The fluorescence quenching of **1** by C_{60}-**2** was estimated to be 49%. The reason is not due to decrease of absorbance of **1** by coexistence of C_{60}-**2** because **1** has a larger absorbance at 570 nm than C_{60}-**2** (inset of Fig. 2). Consequently, the decrease of the fluorescence intensity of LMI**1**–C_{60}-**2** was due to the fluorescence quenching by C_{60}-**2**.

It is well-known that the intracellular uptake of liposomes having a cationic surface is much higher than that of liposomes having neutral or anionic surfaces owing to the occurrence of electrostatic interactions in the latter cases.[36,40–42] However, the strong positive charge of the liposomes leads to cell death under dark conditions. Therefore, we used liposomes consisting of DMPC and cationic lipid **3** {9:1 (mol/mol)} for the subsequent experiments.[36,40–42] The hydrodynamic diameters of LMI**1**, LMIC_{60}-**2**, and LMI**1**–C_{60}-**2** were determined to be 138, 141, and 143 nm, respectively, by means of dynamic light scattering measurements (Table 1). These values were approximately constant irrespective of the presence of **1** and C_{60}-**2**. We characterized the surface potentials of the liposomes using zeta (ζ) potential measurements, finding that all liposomes showed similar cationic surfaces because of the addition of 10 mol% cationic lipid **3** (Table 1).[36]

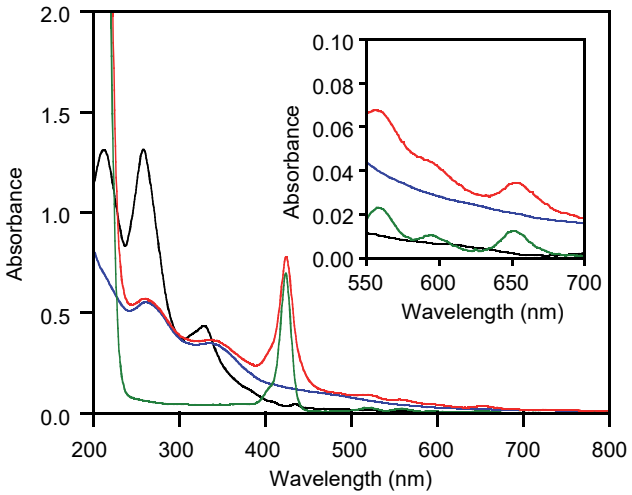

Fig. 2 UV–Vis absorption spectra of γ-cyclodextrin–C_{60}-**2** complex (black), LMI**1** (green), LMIC_{60}-**2** (blue), and LMI**1**–C_{60}-**2** (red) ([DMPC] = 0.1 mM; [**1**]/[DMPC] = 0.0 or 2.5 mol%; [C_{60}-**2**]/[DMPC] = 0.0 or 5.0 mol%) in water. The inset shows the 550–700nm region.

Table 1 Average hydrodynamic diameter (D_{hy}; nm) and ζ potentials (mV) of LMI**1**, LMIC_{60}-**2**, and LMI**1**–C_{60}-**2**.

Liposomes	D_{hy} (nm)[a]	PDI[a,b]	ζ potential (mV)[c]
LMI**1**	137.7 ± 0.9	0.23	+28.3 ± 0.2
LMIC_{60}-**2**	141.3 ± 0.5	0.23	+33.9 ± 2.6
LMI**1**–C_{60}-**2**	142.8 ± 0.3	0.27	+38.5 ± 0.4

[a]The D_{hy} values were determined by conducting dynamic light scattering measurements in Milli-Q water (25 °C). [b]The PDI was calculated using the cumulant method. [c]The ζ potential was measured using capillary cells.

The stability of LMI**1**–C_{60}-**2** in water in the absence and presence of serum protein was evaluated by monitoring the absorbance changes of **1** and C_{60}-**2** in UV–Vis absorption spectra (Fig. 3 and S3). As shown in Fig. 3a and S3a, the absorbance of **1** at 426 nm and that of C_{60}-**2** at 345 nm in LMI**1**–C_{60}-**2** scarcely decreased after incubation in water for 3 d, maintaining over 94% and 98% of the initial values, respectively. However, after 5 d incubation, the absorbance of **1** and C_{60}-**2** in LMI**1**–C_{60}-**2** decreased to 75% and 85%, respectively. The results show that LMI**1**–C_{60}-**2** was slightly unstable in water during prolonged incubation. In contrast, the absorbance of **1** and C_{60}-**2** in LMI**1**–C_{60}-**2** scarcely decreased for 24 h and remained over 88% and 97%, respectively, in blood serum (Fig. 3b and S3b). Therefore, the following cell experiments were performed using LMI**1**–C_{60}-**2** in blood serum.

The photodynamic activities of LMI**1**, LMIC_{60}-**2**, LMI**1**–C_{60}-**2**, and an LMI**1** + LMIC_{60}-**2** mixture containing 10 mol% cationic lipid **3** were evaluated by measuring the viability of murine colon carcinoma cell line (Colon26) and human cervical cancer cell line (HeLa cell). The cell viability was determined as a percent ratio compared with cells untreated with PSs according to the WST-8 method.[43] Dark cytotoxicity toward both cell lines was scarcely observed for LMI**1** and LMI**1**–C_{60}-**2** at concentrations of **1** below 5.0 μM (0 or 10.0 μM for C_{60}-**2**) (Fig. 4a). Furthermore, we confirmed no dark cytotoxicity of LMIC_{60}-**2** at concentrations of C_{60}-**2** below 10 μM toward both cell lines

(Fig. S4). In contrast, the LMI**1** + LMIC$_{60}$-**2** mixture exhibited slight dark cytotoxicity toward both cell lines (Fig. 4a) most likely because it contained twice the amount of DMPC and **3** compared with LMI**1**–C$_{60}$-**2**.[44] Upon light irradiation of the Colon26 and HeLa cells treated with aqueous solutions of LMI**1**, LMIC$_{60}$-**2**, LMI**1**–C$_{60}$-**2**, and the LMI**1** + LMIC$_{60}$-**2** mixture at a wavelength of 610–740 nm for 30 min, the Colon26 and HeLa cell viabilities were reduced in a drug dose–dependent manner (Fig. 4b and S4). The half inhibitory concentrations (IC$_{50}$ values) are summarized in Table 2. The IC$_{50}$ value of LMI**1**–C$_{60}$-**2** toward Colon26 expressed as the concentration of **1** (0.22 μM) was lower than that of LMI**1** (0.56 μM) (Fig. 4b and Table 2). Consequently, the photodynamic activity of LMI**1**–C$_{60}$-**2** was approximately 2.5 times larger than that of LMI**1**. Furthermore, the IC$_{50}$ value of LMI**1**–C$_{60}$-**2** toward Colon26 expressed as the concentration of C$_{60}$-**2** (0.44 μM) was approximately 22 times lower than that of LMIC$_{60}$-**2** (9.62 μM) (Fig. 4b and S4 and Table 2). These results suggested that the photodynamic activity of LMI**1**–C$_{60}$-**2** did not correspond to the sum of that of **1** and C$_{60}$-**2** but stemmed from the synergistic interaction of both components in the composite system. To confirm this hypothesis, we examined the photodynamic activity of a mixture of aqueous solutions of LMI**1** and LMIC$_{60}$-**2** prepared individually. As expected, the IC$_{50}$ value of the LMI**1** + LMIC$_{60}$-**2** mixture ([**1**] = 0.43 μM) was approximately 2.0 times larger than that of LMI**1**–C$_{60}$-**2**.

The IC$_{50}$ value of LMI**1**–C$_{60}$-**2** toward HeLa cells determined as the concentration of **1** (0.13 μM) was approximately 1.7 times smaller than that toward Colon26 cells (0.22 μM) and approximately 2.4 and 1.4 times smaller than that of LMI**1** and the LMI**1** + LMIC$_{60}$-**2** mixture (0.31 and 0.18 μM, respectively) (Fig. 4b and Table 2). Furthermore, the IC$_{50}$ value of LMI**1**–C$_{60}$-**2** toward HeLa cells determined as the concentration of C$_{60}$-**2** (0.25 μM) was approximately 3.6 times lower than that of LMIC$_{60}$-**2** (0.90 μM) (Fig. S4 and Table 2).

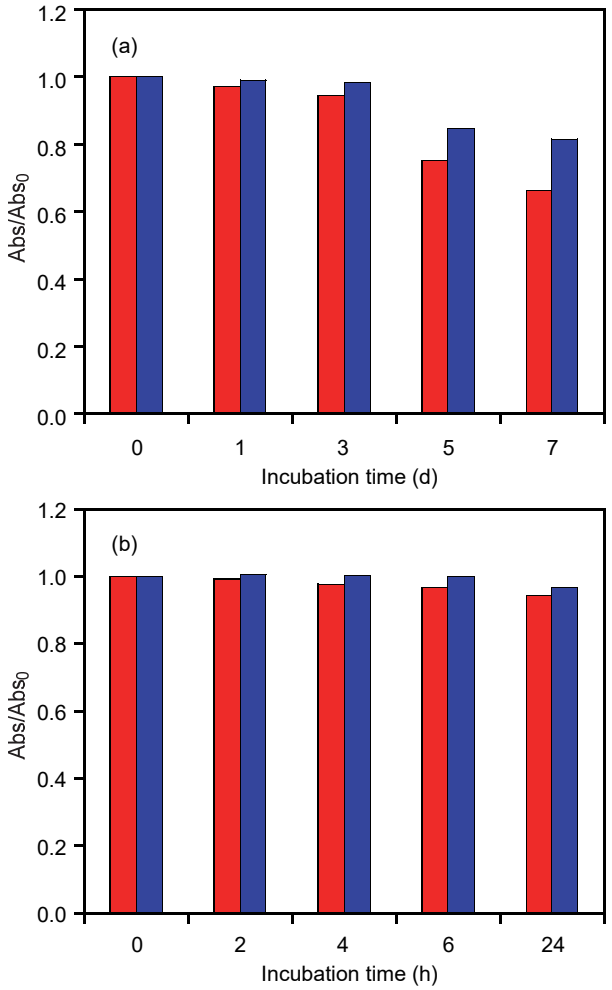

Fig. 3 Changes in the intensity of the absorption maxima of **1** (red) and C$_{60}$-**2** (blue) at 426 and 345 nm, respectively, in LMI**1**–C$_{60}$-**2** (a) in water at 0, 1, 3, 5, and 7 d incubation times and (b) in water in the presence of blood serum at 0, 2, 4, 6, and 24 h incubation times and at 37 °C ([DMPC] = 0.1 mM; [**1**] = 2.5 μM; [C$_{60}$-**2**] = 5.0 μM; 1-cm cell).

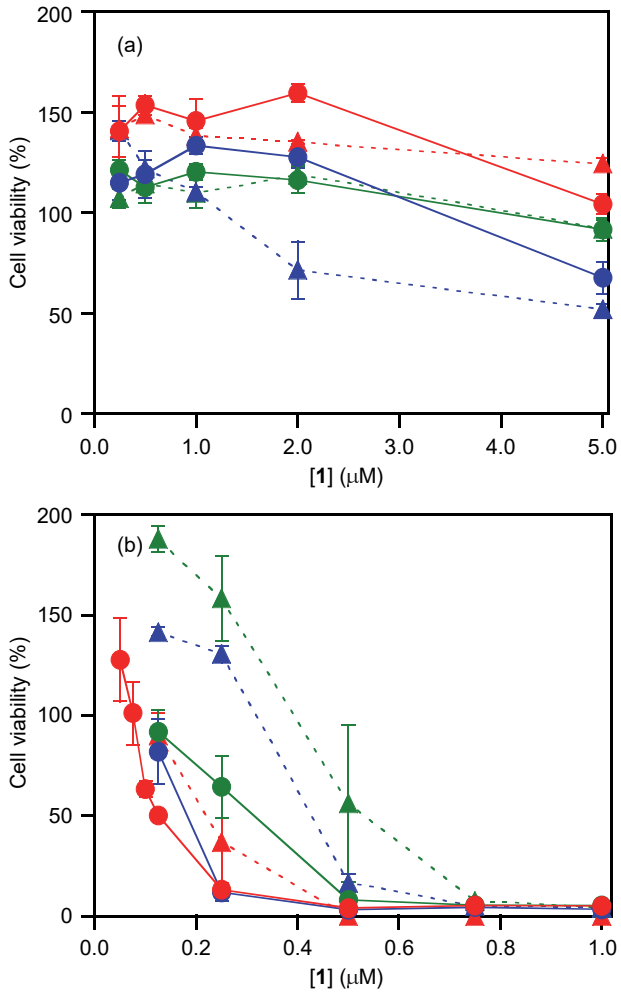

Fig. 4 Cell viability of Colon26 (triangles and dashed lines) and HeLa cells (circles and solid lines) treated with LMI**1** (green), LMI**1**–C$_{60}$-**2** (red), and LMI**1** + LMIC$_{60}$-**2** mixture (blue) (a) in the dark at concentrations of **1** ranging from 0.25 to 1.0 μM and (b) after photoirradiation at 610–740 nm for 30 min at concentrations of **1** ranging from 0.05 or 0.125 to 1.0 μM. The cell viability was evaluated 24 h after treatment using the WST-8 method. Error bars represent the mean ± standard deviation for *n* = 3.

Generally, a selectivity index (SI = IC$_{50}$ in a normal cell line/IC$_{50}$ in a cancer cell line) above 3 indicates a high selectivity toward the cancer cells.[45] The IC$_{50}$ values of LMI**1**–C$_{60}$-**2** toward mouse fibroblasts (L929) as a normal cell line was 0.44 μM

(expressed as [**1**]) (Fig. S5). The SI value of LMI**1**–C_{60}-**2** for Colon26 cells was 2.0, whereas that for HeLa cells was 3.4.

To gain more insight into the high photodynamic activity of the LMI**1**–C_{60}-**2** composite system, the relative ability to generate $^1O_2$ was determined via a chemical method using 9,10-anthracenediylbis(methylene)dimalonic acid (ABDA).[46,47] As shown in Scheme S4, upon the reaction with $^1O_2$, ABDA is converted to an endoperoxide, which decreases its absorbance at 380 nm (Fig. S6). The absorption change of ABDA at 380 nm was plotted against the photoirradiation time for aqueous solutions of LMI**1**, LMIC_{60}-**2**, and LMI**1**–C_{60}-**2** (Fig. 5 and S6). The $^1O_2$ generation ability of LMI**1**–C_{60}-**2** was much higher than that of LMI**1** and LMIC_{60}-**2**, indicating that LMI**1**–C_{60}-**2** worked efficiently as a composite system. In contrast, the increase in the absorption at 560 nm, which is due to the formation of formazan from the reduction of nitroblue tetrazolium by $O_2^{\bullet-}$ (Fig. S7 and Scheme S5), revealed the generation of $O_2^{\bullet-}$.[48] Nevertheless, the ability of LMI**1**–C_{60}-**2** to generate $O_2^{\bullet-}$ was very low irrespective of the absence or presence of β-nicotinamide adenine dinucleotide as an electron donor (Scheme S2).[23] From the high $^1O_2$ generation ability but low $O_2^{\bullet-}$ generation ability of LMI**1**–C_{60}-**2**, it can be inferred that energy transfer from **1** to C_{60}-**2** by type II pathway occurred as the main process governing the photodynamic activity after photoirradiation in the hydrophobic lipid membranes, as is the case of porphyrin–fullerene composite systems in nonpolar solvents (Scheme S2).[2,20,21] Fig. S8 showed that the both energy transfer from photoactivated **1** to C_{60}-**2** and from $^3C_{60}$-**2*** to O_2 can be excepted to occur from the energy levels.

Table 2 IC_{50} values of LMI**1**, LMIC_{60}-**2**, LMI**1**–C_{60}-**2**. and LMI**1** + LMIC_{60}-**2** for Colon26 and HeLa cells.

	IC_{50} for Colon26 (μM)		IC_{50} for HeLa (μM)	
Liposomes	[**1**]^a	[C_{60}-**2**]^b	[**1**]^a	[C_{60}-**2**]^b
LMI**1**	0.56	–	0.31	–
LMIC_{60}-**2**	–	9.62	–	0.90^c
LMI**1**–C_{60}-**2**	0.22	0.44	0.13	0.25
LMI**1** + C_{60}-**2**	0.43	0.86	0.18	0.36

^{a}The IC_{50} values were determined as the concentration of **1**. ^{b}The IC_{50} values were determined as the concentration of C_{60}-**2**. ^{c}The value was reported in ref. 28.

To investigate the reason for the higher photodynamic activity of LMI**1**–C_{60}-**2** toward HeLa cells than toward Colon26 cells (Table 2), the uptake of LMI**1**–C_{60}-**2** was determined by performing a fluorescence-activated cell sorting (FACS) experiment. Colon26 and HeLa cells were incubated for 24 h with a mixture of LMI**1**–C_{60}-**2** ([**1**] = 2.5 μM, [C_{60}-**2**] = 5.0 μM). As shown in Fig. 6 and S9, the intracellular uptake of LMI**1**–C_{60}-**2** by HeLa cells was much higher than that by Colon26, which is consistent with the higher photodynamic activity of LMI**1**–C_{60}-**2** toward HeLa cells. The reason is not clear. In the future, we will try to clarify the reason by investigation of the photodynamic activity toward other cell lines.

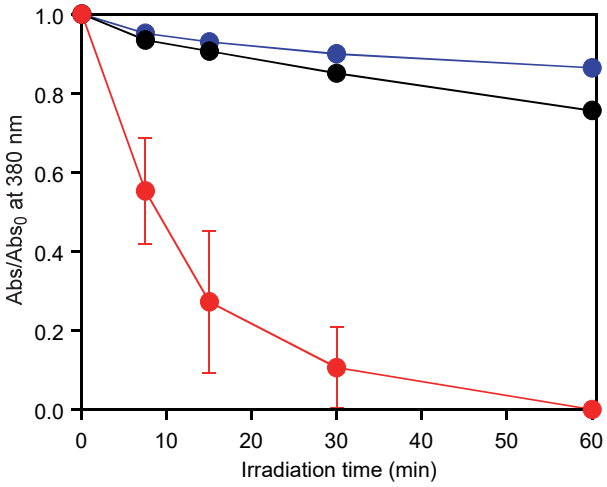

Fig. 5 Time-dependent bleaching of 9,10-anthracenediyl-bis(methylene)dimalonic acid (ABDA) by the singlet oxygen generated from LMI**1** (black), LMIC_{60}-**2** (blue), and LMI**1**–C_{60}-**2** (red) upon photoirradiation (> 620 nm, 15 mW cm^{-2}). A DMSO solution of ABDA was injected into an aqueous solution of liposomes. Changes in the ABDA absorption at 380 nm were monitored as a function of time (Abs_0: initial absorbance) under the conditions of [DMPC] = 0.1 mM, [**1**] = 0 or 2.5 μM, [C_{60}-**2**] = 0 or 5.0 μM, and [ABDA] = 25 μM under an oxygen atmosphere at 25 °C. All data represent the mean values of three independent experiments. Error bars represent the standard deviations.

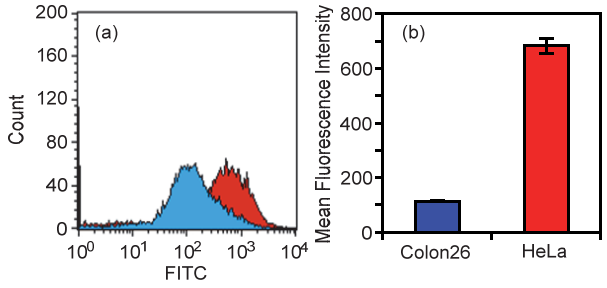

Fig. 6 (a) Flow cytometry analysis for the detection of LMI**1**–C_{60}-**2** in Colon26 (blue) and HeLa (red) cells ([DMPC] = 0.04 mM, [**1**] = 1.0 μM, [C_{60}-**2**] = 2.0 μM). (b) Mean fluorescence intensity of LMI**1**–C_{60}-**2** associated with Colon26 (blue bar) and HeLa (red bar) cells measured after 24 h incubation at 37 °C. Each value represents the mean ± standard deviation of three experiments.

Conclusions

In summary, we successfully prepared an aqueous solution of a relatively stable porphyrin–fullerene (LMI**1**–C_{60}-**2**) composite system. The photodynamic activities of LMI**1**–C_{60}-**2** toward Colon26 and HeLa cells were higher than those of LMI**1**, LMIC_{60}-**2**, and LMI**1** + LMIC_{60}-**2** under photoirradiation at 610–740 nm because LMI**1**–C_{60}-**2** showed much higher $^1O_2$ generation ability than LMI**1** and LMIC_{60}-**2** but very low $O_2^{\bullet-}$ generation ability. The IC_{50} values of LMI**1**–C_{60}-**2** toward Colon26 and HeLa cells were approximately 2.5 and 2.4 times lower than those of LMI**1** as the concentration of **1** and approximately 21 and 3.6 times lower than those of LMIC_{60}-**2** as the concentration of C_{60}-**2**. The results indicate that the energy transfer from **1** to C_{60}-**2** plays a predominant role in the photodynamic process in the hydrophobic lipid membranes, similarly as in nonpolar solvents. Furthermore, the SI values of LMI**1**–C_{60}-**2** for L929/Colon26 cells and L929/HeLa cells were 2.0 and 3.4, respectively, indicating

the high selectivity of LMI**1**–C_{60}-**2** toward HeLa cells. The porphyrin and fullerene composite systems will bring the improvement of the photodynamic activity of other porphyrin derivatives and analogs.

Experimental

Materials

Porphyrin **1**, C_{60}-**2**, and cationic lipid **3** were prepared as described in previously published papers.[49–51] γ-Cyclodextrin was purchased from Wako Pure Chemical Industries Ltd (Tokyo, Japan). 1,2-Dimyristoyl-*sn*-glycero-3-phosphocholine (DMPC) was purchased from Funakoshi Co., Ltd (Tokyo, Japan). 9,10-Anthracenediyl-bis(methylene)dimalonic acid (ABDA) and nitroblue tetrazolium (NBT) were purchased from Sigma-Aldrich (Milwaukee, WI, USA) and Tokyo Chemical Industries Co., Ltd (Tokyo, Japan), respectively. text of the article should appear here with headings as appropriate.

Preparation of liposomes.

DMPC ([DMPC] = 0.10 mM) or a mixture of DMPC and **3** ([DMPC]:[**3**] = 9:1 mol/mol, [DMPC] + [**3**] = 0.10 mM) was dissolved in chloroform (1.0 mL). Subsequently, the solvent was evaporated under a gentle stream of nitrogen, and the residue was further dried under vacuum to remove any solvent traces. The thin lipid films thus obtained were hydrated on the wall of the vial with an appropriate amount of water (1.0 mL) at about 45 °C. The hydrated materials were subjected to five consecutive freeze–thaw cycles (at −195 °C and 50 °C) to produce unilamellar vesicles, which were extruded 11 times through 0.05 μm pores using a LiposoFast miniextruder sourced from Avestin at a temperature above that of the phase transition. The resulting liposomes were uniform in size and had a diameter of approximately 140 nm.

Preparation of γ-cyclodextrin-C_{60}-2 complex.

Aqueous solutions of the γ-cyclodextrin–C_{60}-**2** complex were prepared as described in previously published papers[38] and diluted to a final concentration of 0.10 mM.

Preparation of LMI1, LMIC_{60}-2, and LMI1-C_{60}-2

A DMSO solution (12.2 μL) of **1** (2.0 mM) was injected into an aqueous solution (1.0 mL) of the DMPC or DMPC–**3** liposomes ([DMPC]:[**3**] = 1:0 or 9:1 mol/mol, [DMPC] + [**3**] = 2.00 mM), and these solutions were mixed for 15 min.[26,33,34] After a 1:10 dilution, the final concentrations of the respective components were [**1**] = 2.5 μM and [lipids] = 0.10 mM ([**1**]/[lipids] = 2.5 mol%). LMIC_{60}-**2** and LMI**1**–C_{60}-**2** were prepared via an exchange reaction between the γ-cyclodextrin–C_{60}-**2** complex and the DMPC liposome or DMPC–**3** liposome and LMI**1** (DMPC or DMPC–**3** liposomes), respectively, as described previously.[35–37] The final concentrations of the relevant components were [C_{60}-**2**] = 5.0 μM, [**1**] = 0 or 2.5 μM and [lipids] = 0.10 mM ([C_{60}-**2**]/[lipids] = 5.0 mol%; [**1**]/[lipids] = 0 or 2.5 mol%).

Spectrophotometric assay

The absorbance spectra of LMI**1**, LMIC_{60}-**2**, and LMI**1**–C_{60}-**2** were recorded using a UV-3600 spectrophotometer (Shimadzu Corporation, Kyoto, Japan). The fluorescence spectra of the liposomes were obtained using an F-2700 fluorescence spectrophotometer (Hitachi Ltd, Tokyo, Japan). The excitation and emission wavelengths were set to 570 and 600–750 nm, respectively.

Dynamic light scattering analysis

The hydrodynamic diameters and the zeta potentials of the liposomes were measured using an electrophoretic light scattering instrument equipped with a laser Doppler system (Zetasizer Nano ZS, Malvern Instruments Ltd, Malvern, UK).

Photodynamic activity experiments

Colon26 and HeLa cells were maintained in CO_2-independent medium (Gibco BRL) supplemented with 10% fetal calf serum at 37°C in 5% CO_2. In the experiments conducted to determine the photodynamic activities of LMI**1**, LMIC_{60}-**2**, LMI**1**–C_{60}-**2**, and a mixture of LMI**1** and LMIC_{60}-**2**, the cells were seeded into 48-well culture plates at a density of 8.55×10^4 cells per well. After being allowed to grow overnight, the cells were incubated with LMI**1**, LMIC_{60}-**2**, LMI**1**–C_{60}-**2**, and a mixture of LMI**1** and LMIC_{60}-**2** for 24 h in the dark. The cells were then washed with phosphate-buffered saline and exposed to light for 30 min at room temperature. Light irradiation was conducted using a xenon lamp (MAX-301, 300 W; Asahi Spectra Co., Ltd, Tokyo, Japan) equipped with a VIS mirror module (385–740 nm) and a long-pass filter with a cutoff at 610 nm. The power of the incident light was 9 mW cm^{-2} (610–740 nm). The viability of the cells was measured as the ratio (%) of the number of viable cells in the treatment groups to the number of viable cells in the untreated group. A WST-8 assay was performed 24 h after photoirradiation using a Cell Counting Kit-8 (Dojindo Laboratories, Kumamoto, Japan) according to the manufacturer's instructions.

Identification of reactive oxygen species

The singlet oxygen generated via the ABDA bleaching method (Sigma-Aldrich Corp.) was detected according to a previously reported method.[46,47] ABDA was used as a dimethyl sulfoxide (DMSO) solution ([ABDA] = 2.50 mM). The final concentrations of **1**, C_{60}-**2**, and ABDA in the mixture were 2.5 (or 0), 5.0 (or 0), and 25 μM, respectively. Oxygen gas was bubbled through the sample solutions for 30 min before the photoirradiation to ensure aerobic conditions. The photoirradiation was performed using a xenon lamp (SX-UID500X, 500 W; Ushio Inc., Tokyo, Japan) equipped with a long-pass filter with a cutoff at 620 nm. The light was cooled by passing it through a water filter. The power of the incident light was 16 mW cm^{-2} (over 620 nm). In contrast, the generation of $O_2^{\bullet-}$ was evaluated via chemical methods using nitroblue tetrazolium (NBT).[48] In this analysis, the concentration of C_{60}-**2** in LMI**1**–C_{60}-**2** was 5.0 μM (2760 μL) and that of a DMSO solution of NBT was 0.25 mM (240 μL). As a

positive control, β-nicotinamide adenine dinucleotide (NADH) was added to an aqueous solution of LMI**1**–C_{60}-**2** (final concentration: [NADH] = 0.50 mM). Prior to photoirradiation, oxygen was bubbled through the samples for 30 min to generate the necessary aerobic conditions. Photoirradiation was performed using a xenon lamp (SX-UID500X, 500 W; Ushio Inc., Tokyo, Japan) equipped with a long-pass filter with a cutoff at 620 nm. The power of the incident light was 16 mW cm^{-2} (over 620 nm).

Flow cytometry analysis

Colon26 or HeLa cells (1.0×10^5 cell per well) were incubated with LMI**1**–C_{60}-**2** ([DMPC] = 0.04 mM, [**1**] = 1.0 μM, [C_{60}-**2**] = 2.0 μM) for 24 h at 37 °C in 5% CO_2. Then, the cells were washed with phosphate-buffered saline (PBS), detached with a 0.05% trypsin/0.02% ethylenediaminetetraacetic acid–PBS solution and subsequently suspended in PBS. The suspended cells were added directly to a FACSCalibur flow cytometer (Becton–Dickinson, Franklin Lakes, NJ, USA). The analyses were gated to include single cells on the basis of forward and side light scattering and were based on the acquisition of data from 10000 cells. Log fluorescence values were determined and displayed as single-parameter histograms. The geometric mean fluorescence intensity was calculated using the CellQuest 3.0 program (Becton–Dickinson, Franklin Lakes, NJ, USA).

Author contributions

K. Nishimura: most of the experimental work. K. Yamana: some of the experimental work. R. Kawasaki: discussion and funding acquisition. A. Ikeda: conceptualization, funding acquisition, supervision, and writing of the manuscript

Conflicts of interest

There are no conflicts to declare.

Acknowledgements

This work was supported by ACT-X (R. K., JPMJAX2225), Life Phenomena and Materials, from Japan Science and Technology Agency, by the Japan Society for the Promotion of Science, KAKENHI (R. K., JP19K15401 and JP22K18196) and Research Fellowship for Young Scientist (K. Y., 22J20442). The authors would like to thank Enago (www.enago.jp) for the English language review.

Notes and references

1 H. Imahori, K. Tamaki, D. M. Guldi, C. Luo, M. Fujitsuka, O. Ito, Y. Sakata and S. Fukuzumi, *J. Am. Chem. Soc*., 2001, **123**, 2607–2617.
2 D. M. Guldi, *Chem. Soc. Rev*., 2002, **31**, 22–36.
3 M. E. El-Khouly, O. Ito, P. M. Smith and F. D'Souza, *J. Photochem. Photobiol. C,* 2004, **5**, 79–104.
4 P. D. W. Boyd and C. A. Reed, *Acc. Chem. Res*., 2005, **38**, 235–242.
5 J.-F. Nierengarten, *Eur. J. Inorg. Chem*., **2019**, *2019*, 4865–4878.
6 F. D'Souza and O. Ito, *Coord. Chem. Rev.*, 2005, **249**, 1410–1422.
7 A. L. Schumacher, A. S. D. Sandanayaka, J. P. Hill, K. Ariga, P. A. Karr, Y. Araki, O. Ito and F. D'Souza, *Chem. Eur. J*., 2007, **13**, 4628–4635.
8 H. Imahori, H. Norieda, H. Yamada, Y. Nishimura, I. Yamazaki, Y. Sakata and S. Fukuzumi, *J. Am. Chem. Soc.,* 2001, **123**, 100–110.
9 H. Yamada, H. Imahori, Y. Nishimura, I. Yamazaki, T. K. Ahn, S. K. Kim, D. Kim and S. Fukuzumi, *J. Am. Chem. Soc*., 2003, **125**, 9129–9139.
10 A. Ikeda, T. Hatano, S. Shinkai, T. Akiyama and S. Yamada, *J. Am. Chem. Soc.,* 2001, **123**, 4855–4856.
11 A. Ikeda, T. Hatano, T. Konishi and S. Shinkai, *Tetrahedron,* 2003, **59**, 3537–3540.
12 J. Yang, J. Jing and Y. Zhu, *Adv. Mater*., 2021, **33**, 210102.
13 L. Liu, X. Chen, Y. Chai, W. Zhang, X. Liu, F. Zhao, Z. Wang, Y. Weng, B. Wu, H. Geng, Y. Zhu and C. Wang, *Chem. Eng. J*., 2022, **444**, 1336621.
14 M. E. Milanesio, M. G. Alvarez, V. Rivarola, J. J. Silber and E. N. Durantini, *Photochem. Photobiol*., 2005, **81**, 891–897.
15 C. Constantin, M. Neagu, R. M. Ion, M. Gherghiceanu and C. Stavaru, *Nanomedicine,* 2010, **5**, 307–317.
16 M. B. Ballatore, M. B. Spesia,M. E. Milanesio and E. N. Durantini, *Eur. J. Med. Chem*., 2014, **83**, 685–694.
17 A. Y. Rybkin, A. Y. Belik, N. S. Goryachev, P. A. Mikhaylov, O. A. Kraevaya, N. V. Filatova, I. I. Parkhomenko, A. S. Peregudov, A. A. Terent'ev, E. A. Larkina, A. F. Mironov, P. A. Troshin and A. I. Kotelnikov, *Dyes Pigm.,* 2020, **180**, 108411.
18 K. Sugikawa, K. Masuda, K. Kozawa, R. Kawasaki and A. Ikeda, *RSC Adv*., 2021, **11**, 1564–1568.
19 A. Y. Belik, A. Y. Rybkin, N. S. Goryachev, A. P. Sadkov, N. V. Filatova, A. G. Buyanovskaya, V. N. Talanova, Z. S. Klemenkova, V. S. Romanova, M. O. Koifman, A. A. Terentiev and A. I. Kotelnikov, *Spectrochim. Acta Part A Mol. Biomol. Spectrosc*., 2021, **260**, 119885.
20 A. A. Strelnikov, A. S. Konev, O. V. Levin, A. F. Khlebnikov, A. Iwasaki, K. Yamanouchi and N. V. Tkachenko, *J. Phys. Chem. B,* 2020, **124**, 10899–10912.
21 N. Armaroli, G. Marconi, L. Echegoyen, J.-P. Bourgeois and F. Diederich, *Chem. Eur. J*., 2000, **6**, 1629–1645.
22 C. S. Foote, *Photochem. Photobiol*., 1991, **54**, 659–659.
23 I. Nakanishi, S. Fukuzumi, T. Konishi, K. Ohkubo, M. Fujitsuka, O. Ito and N. Miyata, *J. Phys. Chem. B,* 2002, **106**, 2372–2380.
24 S. Hino, R. Funada, K. Sugikawa, K. Koumoto, T. Suzuki, T. Nagasaki and A. Ikeda, *Photochem. Photobiol. Sci*., 2019, **18**, 2854–2858.
25 S. Hino, R. Funada, K. Sugikawa, R. Kawasaki, K. Koumoto, T. Suzuki, T. Nagasaki and A. Ikeda, *ChemMedChem,* 2021, **16**, 793–803.
26 K. Nishimura, R. Shimada, K. Yamana, R. Kawasaki, T. Nakaya and A. Ikeda, *ChemMedChem*, **2022**, 17, e202200070.
27 A. Ikeda, T. Mae, M. Ueda, K. Sugikawa, H. Shigeto, H. Funabashi, A. Kuroda and M. Akiyama, *Chem. Commun*., 2017, **53**, 2966–2969.
28 R. Shimada, S. Hino, K. Yamana, R. Kawasaki, T. Konishi and A. Ikeda, *ACS Med. Chem. Lett*., 2022, **13**, 641–647.
29 A. Ikeda, M. Akiyama, T. Ogawa and T. Takeya, *ACS Med. Chem. Lett*., 2010, **1**, 115–119.
30 D. Antoku, S. Satake, T. Mae, K. Sugikawa, H. Funabashi, A. Kuroda and A. Ikeda, *Chem. Eur. J.,* 2018, **24**, 7335–7339.
31 D. Antoku, K. Sugikawa and A. Ikeda, *Chem. Eur. J*., 2019, **25**, 1854–1865.
32 R. Kawasaki, D. Antoku, R. Ohdake, K. Sugikawa and A. Ikeda, *Nanoscale Adv*., 2020, **2**, 4395–4399.

33 M. Pons, M. Foradada and J. Estelrich, *Int. J. Pharmacol*., 1993, **95**, 51–56.
34 A. Ikeda, K. Ashizawa, Y. Tsuchiya, M. Ueda and K. Sugikawa, *RSC Adv*., 2016, **6**, 78505–78513.
35 A. Ikeda, T. Sato, K. Kitamura, K. Nishiguchi, Y. Sasaki, J. Kikuchi, T. Ogawa, K. Yogo and T. Takeya, *Org. Biomol. Chem*., 2005, **3**, 2907–2909.
36 A. Ikeda, Y. Doi, K. Nishiguchi, K. Kitamura, M. Hashizume, J. Kikuchi, K. Yogo, T. Ogawa and T. Takeya, *Org. Biomol. Chem*., 2007, **5**, 1158–1160.
37 A. Ikeda, Y. Doi, M. Hashizume, J. Kikuchi and T. Konishi, *J. Am. Chem. Soc*., 2007, **129**, 4140–4141.
38 A. Ikeda, A. Hirata, M. Ishikawa, J. Kikuchi, S. Mieda and W. Shinoda, *Org. Biomol. Chem*., 2013, **11**, 7843–7851.
39 A. Ikeda, T. Iizuka, N. Maekubo, R. Aono, J. Kikuchi, M. Akiyama, T. Konishi, T. Ogawa, N. Ishida-Kitagawa, H. Tatebe and K. Shiozaki, *ACS Med. Chem. Lett*., 2013, **4**, 752–756.
40 C. R. Miller, B. Bondurant, S. D. McLean, K. A. McGovern and D. F.O'Brien, *Biochemistry,* 1998, **37**, 12875–12883.
41 M. Akiyama, A. Ikeda, T. Shintani, Y. Doi, J. Kikuchi, T. Ogawa, K. Yogo, T. Takeya and N. Yamamoto, *Org. Biomol. Chem*., 2008, **6**, 1015–1019.
42 Y. Doi, A. Ikeda, M. Akiyama, M. Nagano, T. Shigematsu, T. Ogawa, T. Takeya and T. Nagasaki, *Chem. Eur. J*., 2008, **14**, 8892–8897.
43 H. Tominaga, M. Ishiyama, F. Ohseto, K. Sasamoto, T. Hamamoto, K. Suzuki and M. Watanabe, *Anal. Commun*., 1999, **36**, 47–50.
44 E. Yoshihara and T. Nakae, *Biochim. Biophys. Acta*, 1986, **854**, 93–101.
45 P. Prayong, S. Barusrux and N. Weerapreeyakul, *Fitoterapia*, 2008, **79**, 598–601.
46 N. A. Kuznetsova, N. S. Gretsova, O. A. Yuzhakova, V. M. Negrimovskii, O. L. Kaliya and E. Luk'yanets, *Russ. J. Gen. Chem*., 2001, **71**, 36–41.
47 A. Ikeda, M. Akiyama, K. Sugikawa, K. Koumoto, Y. Kashijima, J. Li, T. Suzuki and T. Nagasaki, *Org. Biomol. Chem*., 2017, **15**, 1990–1997.
48 Y. Yamakoshi, N. Umezawa, A. Ryu, K. Arakane, N. Miyata, Y. Goda, T. Masumizu and T. Nagano, *J. Am. Chem. Soc.,* 2003, **125**, 12803–12809.
49 D. A. James, D. P. Arnold and P. G. Parsons, *Photochem. Photobiol*., 1994, **59**, 441–447.
50 M. Maggini, A. Karlsson, L. Pasimeni, G. Scorrano, M. Prato and L. Valli, *Tetrahedron Lett*., 1994, **35**, 2985–2988.
51 Y. Murakami, A. Nakano, A. Yoshimatsu, K. Uchitomi and Y. Matsuda, *J. Am. Chem. Soc*., 1984, **106**, 3613–3623.